GeoHazards

MDPI

Review

Rockfall Volume–Cumulative Frequency Relationships for Rockfall Hazard Quantification Using Historical and Change Detection Data

Swarna Bhowmick * and Renato Macciotta

Department of Civil and Environmental Engineering, University of Alberta, Edmonton, AB T6G 2R3, Canada; macciott@ualberta.ca

* Correspondence: bhowmic1@ualberta.ca

Abstract

Rockfall records for hazard assessments commonly present rockfall volume–cumulative frequency curves based on observations of rockfall occurrences that are noticed at or in the vicinity of infrastructure. These curves are in log–log scale, where the curves for larger volumes are fitted to a power law (linear fit in the log–log plot). The slope of this linear fit in log–log plots has been qualitatively attributed to rock mass characteristics (lithology, rock mass quality, discontinuities); however, there are not many direct insights that greenfield sites (new sites or areas with scarce to no data) could adopt for an order-of-magnitude estimation of rockfall hazard. This paper collects data from the literature, past and current, and presents details of these rockfall volume–cumulative frequency curves for different lithologies and rock mass qualities. Importantly, recent databases on rockfall frequency and volumes as obtained through change detection are utilized, which can provide more detailed and less biased rockfall occurrence data.

Keywords: rockfall; volume–cumulative frequency; change detection

1. Introduction

Rockfalls and rockslides represent one of the most common failure mechanisms affecting steep rock slopes in both linear transportation corridors and large open-pit mines. Along highways, rail lines, pipelines, and tunnels, even small-volume rockfalls can cause serious safety hazards, traffic disruptions, and costly maintenance interventions. Rockfalls are extremely rapid processes that, even in the case of small events, exhibit high kinetic energy and damaging capability [1,2]. Rockfalls involve the separation of rock blocks from steep faces with minimal shear along a surface; motion typically begins as free-fall and then transitions to impacts and rolling [3,4]. These rockfalls range from small cobbles to large boulders hundreds of cubic meters in size and travel at speeds ranging from a few to tens of meters per second [5]. Despite extensive research on slope stability, rockfall occurrence remains highly stochastic, controlled by complex interactions among rock mass quality, lithology, weathering, discontinuity networks, and external triggers such as freeze thaw cycles [6], rainfall, poor blasting [7], and long–term degradation. For transportation corridors such as highways, railways, and pipelines, rockfalls pose persistent safety risks, cause operational interruptions, and require significant maintenance expenditures [8]. Similarly, in open-pit mines, rockfalls threaten worker safety, disrupt haulage operations, reduce overall productivity, and can escalate into larger-scale instabilities when not properly char-

Check for updates

Academic Editor: Tiago Miguel Ferreira

Received: 1 April 2026
Revised: 28 May 2026
Accepted: 1 June 2026
Published: 9 June 2026

Copyright: © 2026 by the authors. Licensee MDPI, Basel, Switzerland. This article is an open access article distributed under the terms and conditions of the Creative Commons Attribution (CC BY) license.

acterized [6]. As a result, reliable quantification of rockfall hazards across diverse geological and infrastructure settings continues to be a major requirement.

Accurate assessment of rockfall hazards is therefore essential for informed slope design, risk mitigation, and long-term infrastructure management. Rock slope risk along highways, railways and open pits arise from both frequent small rockfalls and rare large failures, and comprehensive. Risk analyses require understanding their volume–frequency behavior [9]. However, characterizing rockfall frequency and magnitude remains challenging due to the inherently stochastic nature of rockfall processes, observational biases in traditional inventories, and variability in rock mass structure and lithology [10].

Conventional incident-based or field-mapped rockfall databases typically underrepresent small-volume events because they are less observable and often overlooked, leading to incomplete frequency–magnitude distributions and potentially misleading hazard estimations [11].

To address these limitations, rockfall hazard studies increasingly rely on rockfall volume–cumulative frequency (RVC) relationships, expressed as power-law trends in log–log space. The linear slope of the frequency–volume curve (commonly denoted as the b-value) provides insight into the relative abundance of small versus large events and has been shown to correlate with lithology, discontinuity persistence, rock mass quality, and geomorphic processes [10,12]. Recent advances in remote sensing—such as terrestrial laser scanning (TLS), drone-based photogrammetry, and high-resolution LiDAR systems—have enabled detailed detection of rockfall events across entire slope surfaces, including sub-decimeter-scale detachments that are systematically missed in traditional inventories [13]. These change detection datasets dramatically improve the completeness of rockfall catalogs, reduce observational bias, and enhance the statistical reliability of RVC curves. As a result, integrating historical records with modern change detection data provides a more robust basis for hazard quantification, supports better identification of lithology-dependent behaviors, and strengthens predictive assessments at both existing sites and new greenfield locations with limited monitoring histories.

This paper summarizes the statistical relationship between historical rockfall inventories and change detection datasets by analyzing the slopes of their log–log volume–cumulative frequency curves (b-values), updating existing inventories with recently published case studies. By comparing these RVC relationships, the work seeks to understand how observational bias, lithological variability, and data-collection methods influence rockfall characterization. In addition, the paper evaluates why modern change detection techniques—enabled by high-resolution TLS and photogrammetric workflows—provide a scalable and quantitative framework for rockfall hazard assessment across diverse geological settings. These methods capture small-volume events that are typically missing from historical datasets, thereby producing more complete volume–cumulative frequency distributions and improving the robustness of hazard evaluations.

2. Rockfall Volume–Cumulative Frequency Relationships

Rockfall magnitude is most commonly expressed as the volume of displaced material in line with broader landslide studies where magnitude may be represented by either area or volume [14]. Quantitative risk assessment requires estimating the probability or frequency of events across different magnitude classes [15,16], and for rockfalls this is typically achieved through magnitude–frequency analysis [9,17,18]. Event frequencies can be expressed using cumulative or non-cumulative distributions [19], or as frequency densities normalized by bin size [20,21]. Over a defined scale range, (RVC) relationships generally follow a power-law trend, with deviations only at very small and very large volumes.

Following [9], cumulative exceedance of rockfall volumes commonly follows a Gutenberg–Richter-style power law used in seismology [9,22]:

$$\log F = A + b \log(M), \quad (1)$$

where F is the cumulative frequency of events exceeding a given volume M. The constant A is site and time-dependent, while the slope b characterizes the distribution of rockfall frequencies across the study area and its subdivisions. In practice, b-values are obtained by applying linear regression to the straight portions of the power-law segments on log–log RVC plots. The exponent b also provides insight into rockfall size distribution: higher values indicate inventories dominated by small-volume events, whereas lower values reflect a greater proportion of large failures. A compilation of historical rockfall inventories—including lithology, b-values, and associated volume ranges—is summarized in Table 1.

Table 1. Characterization of rock slope failures from historical inventories.

Case No.	Slope Lithology	Slope "b"	R^2	Rockfall Events	Reference	Volume Range
1	Calcareous and quartzitic rock	0.72		409	[23] [a]	10^{-2} to 10 m^3
2	NA NA	0.19 0.23		200 200	[24] [a]	10^{-6} to 10^{6} m^3 10^{-2} to 10^{7} m^3
3	Quartzdiorite to granodiorite	0.43 0.4 0.7 0.646	0.99 0.94 0.95 0.99	389 123 64 122	[9] [b]	0.01 to 10,000 m^3 1 to 10,000 m^3
4	Muddy limestone	0.625		27	[18]	Greater than 1 m^3
5	Limestone and marl	1.2		155- for 9.9×10^{-5} to 2×10^{2} m^3 and 62- for 8.11×10^{-3} to 1.29×10^{2} m^3	[5]	9.9×10^{-5} to 2×10^{2} m^3 and 8.11×10^{-3} to 1.29×10^{2} m^3
6	A mix of sandstone, granodiorrite, pelitic schist, granite gneiss with abundant pegmalite and chert limestone	0.62	0.86	535	[25]	Above 0.6 m^3
7	Granodiorite and hornfels	0.537	0.97	25	[4]	Greater than 1 m^3
8	Granite and volcanic rocks	0.896		201	[26]	Approximately 3 m^3
9	Metamorphic and sedimentary rocks Calcareous cliffs (limestone and marl) Granite cliffs	0.45 ± 0.15 0.41 ± 0.11 0.46 ± 0.11		59 87 101	[27] [c]	1 to 10,000 m^3 0.5 to 106 m^3 1–10^{6} m^3

Table 1. *Cont.*

Case No.	Slope Lithology	Slope "b"	R^2	Rockfall Events	Reference	Volume Range
10	Undifferentiated rock cliffs	0.51 ± 0.07		54	[24] [d]	10^3 to 2 × 10^{10} m^3
	Calcareous cliffs (limestone and marl)	0.41 ± 0.06		87		10^{-2} to 10^6 m^3
	Granite cliffs	0.45 ± 0.06		101		1 to 10^6 m^3
11	Granite cliffs	0.57	0.99	214	[28]	1 to above 10^6 m^3
12	Granite	0.4	0.97	463	[20]	Greater than 50 m^3 (1980–2002 dataset)
13	Granite cliffs	1.07		157	[21] [e]	10^{-3} to 10^3 m^3
	Granite	1.07		135		10^{-1} to 10^6 m^3
	Calcareous	1.07		89		10 to 10^6 m^3

[a] Taken from [27], and from [24]. [b] Provides the value for Highway 99, BCR, Highway 1 and CP, respectively. [c] Provides the values for Upper Arly Gorges, French Alps, Grenoble, French Alps, and Yosemite Valley, California, respectively. [d] Provides values for Worldwide Inventory, Grenoble, France, and Yosemite, California, respectively. [e] Provides values for Umbria-Marche, Yosemite, California, and Grenoble, French Alps, respectively.

Many landslide datasets exhibit a decrease in frequency at the smallest magnitudes—commonly referred to as the "rollover" [21]—where the inverse power-law scaling is no longer valid. To represent this curvature, alternative statistical models such as the double-Pareto [19,29] and inverse-gamma distributions [5,21] are often employed. These deviations have been attributed to physical minimum-event sizes, mechanical constraints, or censoring effects associated with limited monitoring resolution [19,30–32].

Change Detection

Change detection analyses, using multi-temporal high-resolution point-cloud models of slope surfaces, enable the identification of active instability zones and the quantitative characterization of rockfall magnitude, frequency, and spatial distribution. Ref. [33] demonstrated that terrestrial laser scanning (TLS)-derived change maps can characterize rockfall source zones, failure mechanisms, and bench-scale fragmentation processes in mining environments. Recent studies have explored multisensory change detection by combining UAV–based photogrammetry with TLS or aerial LiDAR to improve areal coverage and temporal sampling [34]. These hybrid approaches allow frequent monitoring at high spatial resolution, making it possible to characterize both small, frequent events and larger, more infrequent rockfalls over broad slope extents. Change detection has therefore emerged as a scalable and quantitative framework for rockfall hazard assessment, enabling more complete inventories, improved magnitude–frequency analysis, and better-informed risk management.

Change detection from sequential terrestrial laser scanning (TLS) surveys have demonstrated strong capability for quantifying rockfall detachment volumes and identifying patterns of pre-failure deformation through direct point-cloud differencing, providing insight into spatially clustered failure processes [12]. Subsequent methodological advances focused on reducing noise, improving alignment accuracy, and filtering spurious measurements, thereby enabling more reliable detection of small-volume rockfalls that are commonly underrepresented in traditional inventories [11]. Such accurate 3D change detection in geomorphic environments requires careful consideration of complex topography, surface roughness, occlusion effects, and registration uncertainty when comparing multi-temporal point-cloud datasets.

Ref. [35] further showed that TLS-derived datasets follow a power-law distribution for event volumes greater than approximately 0.03 m^3, enabling consistent estimation of b-values for small and medium magnitudes. A consolidated set of b-values, lithologies, and associated TLS observations from change detection studies are presented in Table 2.

Table 2. Characterization of rock slope failures from change detection observation.

Case No.	Slope Lithology	Slope "b"	R^2	Rockfall Events	Reference	Volume Range (m^3)
1	Basaltic cliff	1		370	[27] [1]	
2	Quartzofeldspathic gneiss	1.01	0.99	1982	[35]	0.03 to 45 m^3
3	Limestone cliff	0.75 ± 0.04	0.99	344	[36]	Greater than 0.05 m^3
4	Feldspathic sandstone	0.43	0.81	100	[37] [2]	Above or equal to 1 m^3
	Sandstone	0.663	0.85			
	Paleozoic and dolomitic limestones	0.682	0.93	31		
5	Siltstone/Sandstone and basaltic	0.555	0.99	592	[38]	Greater than 0.003 m^3
6	Limestone and marl	0.463	0.92	118	[39]	For all volume data (9.55 to 7.63 m^3)
		0.676	0.97			Volumes greater than 0.1 m^3
7	Granodiorites	0.922	0.99	375 discontinuity surfaces	[40]	Greater than 0.25 m^3
8	Upper cretaceous chalk	0.54	0.99	8582 eroded patches	[41]	

[1] Taken from [27]. [2] Values for C018, S020 and S042, respectively.

3. Selected Case Study Discussion

In recent years, for rockfall hazard assessment in transportation corridors and open pits, remote sensing has become a very well-known and widely practiced technique. Conventional remote monitoring methods include terrestrial and satellite-based Interferometric Synthetic Aperture Radar (InSAR), Light Detection and Ranging (LiDAR) methods (also referred to as laser scanning), photogrammetry, and traditional total stations paired with survey monuments [42–44]. Some geological formations and rock slopes occur in remote or inherently dangerous environments, posing significant challenges and safety risks for collecting rockfall data and conducting on-site monitoring. Under these conditions, remote sensing methods allow surveyors to acquire detailed measurements while remaining safely away from bench faces, thereby minimizing exposure to rockfall, raveling, and other hazardous slope processes. The remote sensing technologies like photogrammetry and LiDAR are beneficial for quantifying rockfalls as they can provide high resolution and high 3D point-cloud representations of slope, while eliminating worker exposure to hazard [45,46].

3.1. Case Studies

This section presents more detailed examples for a subset of the case studies used in our study. These examples aim to show the typical settings and processes utilized to obtain the rockfall datasets. Further details in other case studies can be accessed through the references cited in this paper.

3.1.1. Change Detection of Limestone Cliff Mountain Using TLS

On the high limestone cliffs of Mont Saint-Eynard (1308 m), located 4 km north of the Grenoble city center (Figure 1), repeated TLS surveys detected over 300 rockfall events with volumes exceeding 0.05 m^3. Across a rock wall measuring approximately 750 × 200 m, the cumulative power-law distribution yielded an exponent slope of b = 0.75 ± 0.04 [36]. When compared with a historical rockfall inventory compiled over 120 km of predominantly massive limestone, a lower power-law exponent of b = 0.69 ± 0.07 was observed for events with volumes greater than 0.2 m^3. This discrepancy indicates that smaller events (V < 0.2 m^3) are systematically underrepresented in traditional inventories, primarily due to visibility constraints and limited temporal coverage. For example, Figure 2 illustrates the cumulative rockfall volume–frequency distributions derived from TLS for events exceeding 0.2 m^3 and 0.05 m^3 respectively.



Figure 1. Photograph of the Mont Saint–Eynard cliff from [36].

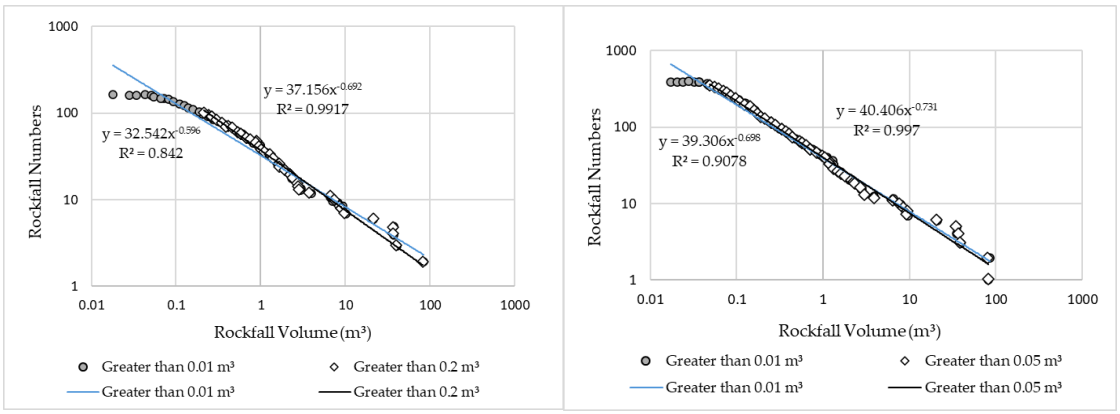

(**a**) (**b**)

Figure 2. (**a**) Rockfall volume–frequency curve for volumes greater than 0.2 m^3. (**b**) Rockfall volume–frequency curve for volumes greater than 0.05 m^3 based on the data from [36].

These results demonstrate that TLS–based change detection substantially improves the completeness of rockfall inventories, particularly for small-volume events that are difficult to detect through conventional field mapping. Consequently, remote sensing methods such as TLS provide significant advantages for rockfall frequency characterization and hazard assessment on large and inaccessible cliff faces.

3.1.2. Change Detection of Rockfall Activity Using TLS at the White Canyon, British Columbia

At White Canyon (CN Ashcroft rail corridor, BC) (Figure 3), multi-epoch TLS revealed approximately 1982 rockfall events with volumes ranging from ≈0.01–45 m^3 for over

~15 months. Figure 4 illustrates that for volumes V > 0.03 m^3 the cumulative frequency follows a power law with b ≈ 1.0, reflecting dominance of small detachments consistent with gneissic fragmentation [35].

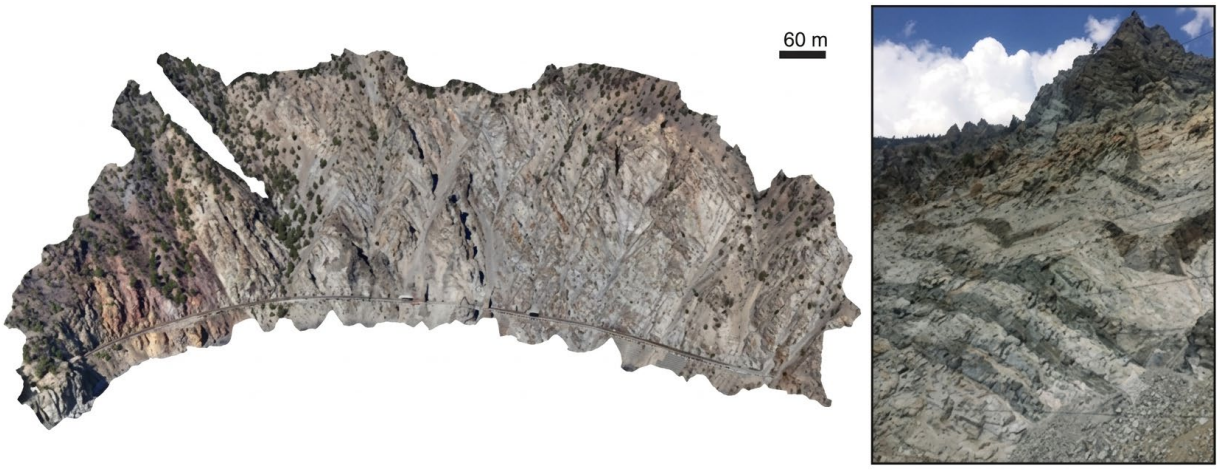

Figure 3. White Canyon West slope photogrammetry model and image taken from track level from [35].

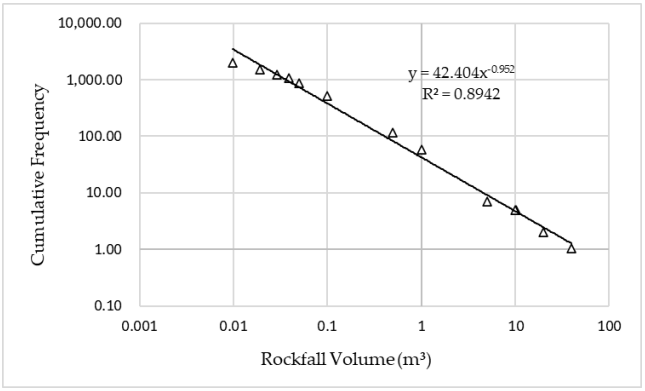

Figure 4. Rockfall volume–frequency curve of rockfall rates based on the data from [35].

The study further demonstrated that the temporal spacing of TLS scans has a direct effect on rockfall detectability. As the duration between scans increases, individual events begin to spatially overlap, particularly for small-volume detachments, resulting in underestimation of event counts and distortion of the rollover region in the frequency–magnitude curve [35]. These findings underscore the importance of selecting appropriate scan intervals for reliable rockfall monitoring. This approach provides a robust framework for quantitative hazard assessment, enabling improved characterization of rockfall activity along critical transportation corridors.

3.1.3. Change Detection of Coastal Chalk Cliffs Using TLS (Mesnil-Val, Normandy)

At Mesnil-Val on the Normandy coast, Ref. [41] conducted six TLS surveys for 2.5 years starting from 2005, capturing high-resolution 3D point clouds of an 850 m long, 20–80 m high chalk cliff section (Figure 5). Successive scans were differenced to derive Digital Surface Model (DSM) changes used for the planar cliff site, enabling precise detection of erosion scars ranging from 10^{-4} to 10^4 m^3.

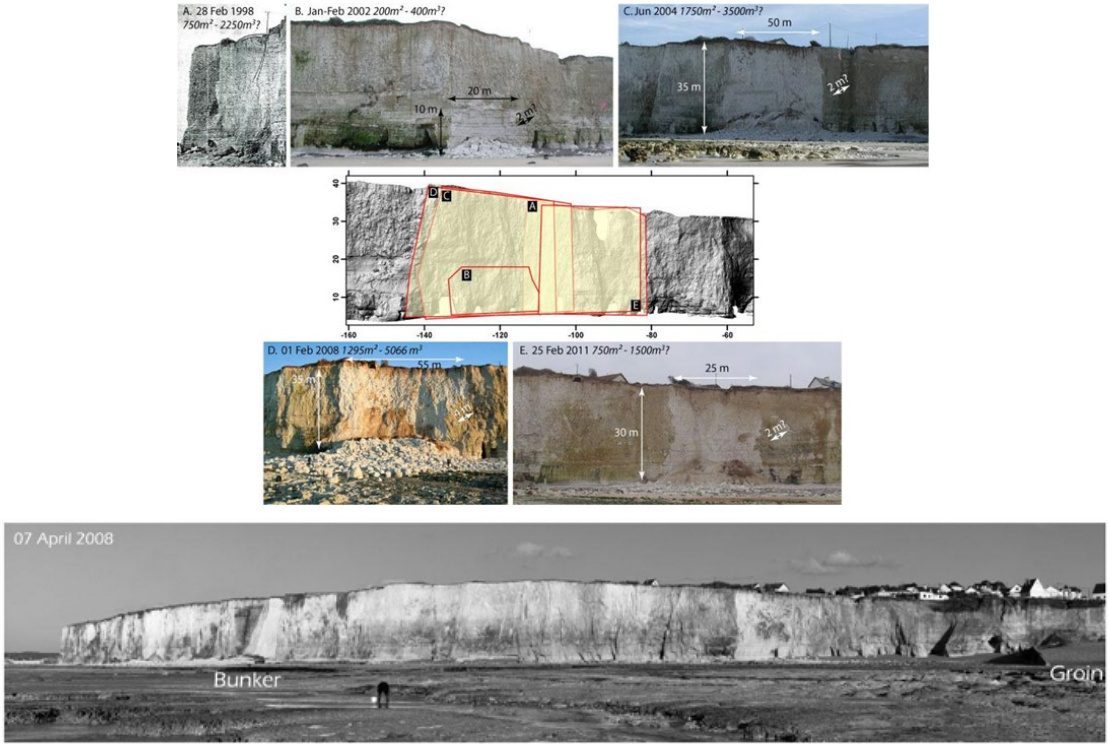

Figure 5. Photograph of Mesnil Val chalk cliff site from front (**below**) and major rockfall scars between 1998–2011 (**above**) from [41]. (panels A–E denote specific rockfall events detailed in the source text).

The resulting inventory exhibits a clear power-law relationship in the cumulative volume–frequency domain of the exponent b−value of 0.54 (Figure 6) and volume ranging from 0.001 to 100 m^3. Linear scaling in log–log space indicates that rockfall volumes follow a self-similar fragmentation process, with complementary cumulative distribution functions (CCDFs) describing exceedance rates. For example, events on the order of 10,000 m^3 for a 40 m × 40 m × 6.25 m chalk mass exhibit return periods of 2.2 years, emphasizing the substantial hazard posed even over short monitoring intervals.

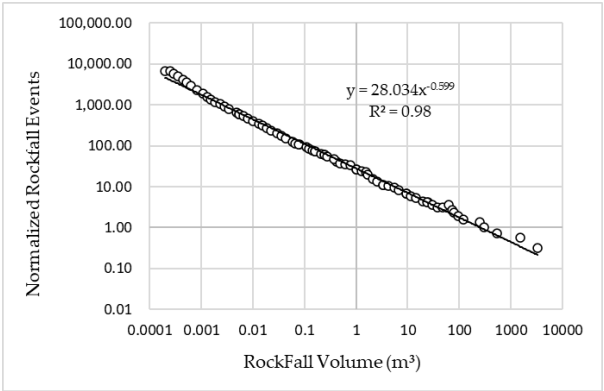

Figure 6. Rockfall volume–frequency curve of rockfall events based on the data from [41].

This case study demonstrates how TLS-derived change detection captures the full spectrum of rockfall magnitudes, overcomes inventory bias against small events, and provides statistically defensible rockfall volume–cumulative frequency (RVC) relationships essential for quantitative hazard assessment.

3.1.4. Rockfall Frequency–Magnitude Assessment for Rockfall Scars at the Forat Negre and Borrassica Slopes in the Eastern Pyrenees Using Change Detection

A rockfall scar is defined as the rupture surface exposed on a vertical cliff following one or multiple rockfall events. Ref. [40] developed a six−step TLS-based workflow to identify detached rockfall source areas and to compute the volume distribution of rockfall scars using repeated terrestrial laser scanning surveys conducted at the Forat Negre and Borrassica slopes in the Eastern Pyrenees (Figure 7). Change detection through direct differencing of successive TLS point clouds enabled accurate delineation of newly exposed cliff surfaces and quantification of volumetric losses, including small-scale failures that are commonly underrepresented in conventional field inventories.



Figure 7. Location of the pilot zone (yellow) and partial view of the Forat Negre and Borrassica slopes in the Solà d'Andorra from [40].

Rockfall scars with volumes greater than 0.25 m^3 were analyzed using cumulative volume–frequency relationships plotted in log–log space. The resulting distribution was well described by a power-law function with an exponent b = 0.9 (Figure 8), consistent with fragmentation-controlled rockfall processes reported in previous studies. This exponent provides quantitative insight into the relative occurrence of small versus large rockfall events and serves as an indicator of the structural fabric of the rock mass.

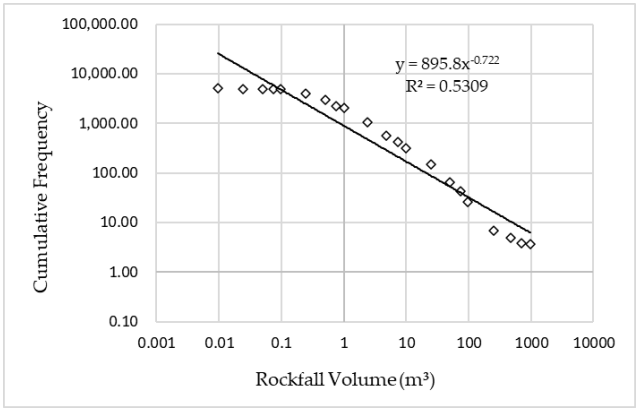

Figure 8. Rockfall volume–frequency curve of rockfall scars based on the data from [40].

The results demonstrate that, in the absence of complete rockfall inventories, scar-based magnitude–frequency relationships can be used as a proxy for rockfall activity, provided certain assumptions are satisfied: (i) rockfall volume is equivalent to the measured scar volume, and (ii) large-scale failures involving sliding along discontinuity planes are considered only where joint spacing is below a defined threshold (20 cm in this case) and the planes are laterally continuous.

3.1.5. Change Detection Based on Rock Slope Assessment Along Transportation Corridors

Wollenberg-Barron [37] investigated the relationship between rockfall volumes obtained from change detection analysis and established condition assessment tools used for transportation corridors in three different sites (C018, S020 and S042) in Canada to support capital expenditure prioritization under a geotechnical asset management framework (Figure 9). Multi-temporal remote sensing datasets acquired using ground-based LiDAR and UAV-based photogrammetry were processed using cloud-to-cloud and M3C2 change detection techniques to identify individual rockfall detachments and quantify volumetric loss at three representative rock slope sites (Figure 10). Rockfall events with volumes greater than or equal to 1 m^3 were used to develop cumulative volume–frequency (V–F) curves, enabling direct linkage between measured rockfall activity and slope performance metrics, including Alberta Transportation's GRMP performance factor rating, Rockfall Hazard Rating System (RHRS), Q-slope classification, and Geological Strength Index (GSI) [37].

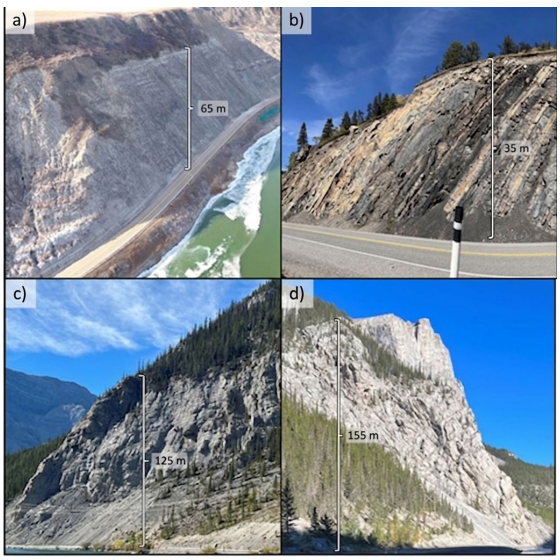

Figure 9. Photograph of (**a**) C018, (**b**) S020, (**c**) S042–North and (**d**) S042–South sites from [37].

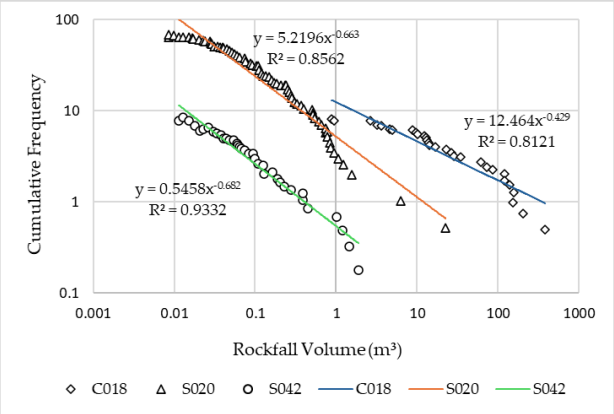

Figure 10. Cumulative frequency of detected volume changes from the active zones of three sites (C018, S020 and S042) based on the data from [37].

The results demonstrate that observational engineering geology parameters, such as weathering intensity and fracture frequency, when appropriately calibrated, can be used to approximate expected rockfall hazard levels. The study also highlights that scan frequency and detection thresholds strongly influence the lower bound of the volume–frequency distribution, underscoring the importance of consistent monitoring strategies. By integrating quantitative volume–frequency analysis with condition assessment tools, the proposed change detection framework provides transportation agencies with a more objective and defensible basis for prioritizing slope mitigation and maintenance compared to reliance on qualitative assessments alone.

4. Study Limitations

While this study provides a comparative analysis of RVC characteristics across diverse lithologies, several inherent limitations should be acknowledged. Several factors can bias change detection results and limit inventory completeness. The primary constraint is the finite availability of high-resolution change detection datasets, which influence statistical robustness and prevent definitive global conclusions. Furthermore, the synthesis is subject to heterogeneities in the source data, including varying monitoring durations, disparate reporting criteria, and inconsistent detection thresholds across the literature. Adverse weather, poor lighting, and dense vegetation can obscure the ground surface or degrade data quality. Additionally, surface roughness often creates 'shadows' or occlusions, leading to missing data [37,47]. These environmental constraints, combined with equipment limits like point density and scan intervals, can result in the underreporting of small rockfall events, ultimately affecting the calculated b-value. These factors introduce a degree of aleatory uncertainty that must be considered when extrapolating these results to greenfield sites.

5. Review of RVC Relationships—B-Values and Rollover

Although the limited number of available studies currently restricts definitive conclusions from a comparative study between RVC characteristics for different lithologies and rockfall database acquisition methods, important observations shed insight into rockfall behavior under diverse settings. The analysis is based on site-specific lithological characteristics, the slope b of the volume–cumulative frequency relationships in log–log space, and the behavior of the rollover region. By examining how change detection-derived inventories influence the estimation of b-values and reduce the extent of the rollover region, this discussion highlights the improved capability of change detection to cap-

ture frequent small-volume rockfalls that are typically underrepresented in traditional observational datasets.

5.1. Site Lithology

Site lithology encompasses rock type, associated with its geological formation and geographic location. Lithology and climate of the area will define the weathering characteristics of rock slopes and cliffs. Variations in rock slope behavior are strongly controlled by lithological factors, which influence rock mass strength, fracture characteristics, and failure mechanisms [35].

To evaluate the influence of lithology on RVC relationships, we used the set of datasets derived from both historical rockfall inventories and change detection analyses assembled (Tables 1 and 2). Two complementary analyses were conducted to compare results obtained from historical inventories with those derived from change detection. For each dataset, statistical box plots were constructed for different lithologies using the power-law exponent b obtained from the RVC relationships (Table 3). This approach enables systematic comparison of the distribution, variability, and central tendency of b-values across lithologies and data sources, providing insight into how inventory type and rock mass characteristics jointly influence observed RVC relationships and rockfall frequency–magnitude behavior.

Table 3. Number of historical studies b-values and rockfall events for each lithology.

Rockfall Events	Limestone	Granite	Quartzdiorite to Granodiorite	Others [1]
	0.72	0.896	0.43	0.19
	0.625	0.46	0.4	0.23
	1.2	0.45	0.7	0.51
	0.41	0.57	0.646	0.45
	0.41	0.4	0.62	
	1.07	1.07	0.537	
		1.07		
Total	916	1372	1258	513

[1] The group "Other" represents the slope lithologies of non-identified ([24]), metamorphic and sedimentary rocks ([27]) and undifferentiated rock cliffs ([24]).

A key limitation of this study is the uneven distribution of datasets across lithologies, as summarized in Table 3. While granite and limestone are comparatively well represented, fewer case studies are available for quartz diorite–granodiorite and metamorphic–sedimentary lithologies, reducing the statistical robustness of lithology-specific comparisons. Consequently, trends for underrepresented lithologies should be interpreted with caution. Continued application of change detection techniques is expected to expand available datasets and improve the reliability of lithology-dependent rockfall frequency–magnitude analyses.

Figure 11 illustrates the relationship between site lithology and the power-law slope b derived from historical rockfall inventories. The results indicate that quartz diorite to granodiorite lithologies and the group labeled "Others" exhibit relatively narrow and clustered distributions of b-values, while limestone and granite display a wider range and greater variability, with values spanning approximately from 0.4 to 1.2.

The broader spread observed for limestone and granite indicates greater heterogeneity in rockfall fragmentation processes, likely driven by variations in bedding, jointing, and weathering. These lithologies exhibit positively skewed, non-symmetrical distributions, reflecting inventories dominated by frequent small-magnitude events with occasional larger failures. In contrast, the tighter distributions associated with quartz diorite–granodiorite and the "Others" group may suggest more uniform behavior; however, this reduced

variability could be attributable to the limited number of available case studies rather than intrinsic lithological controls.

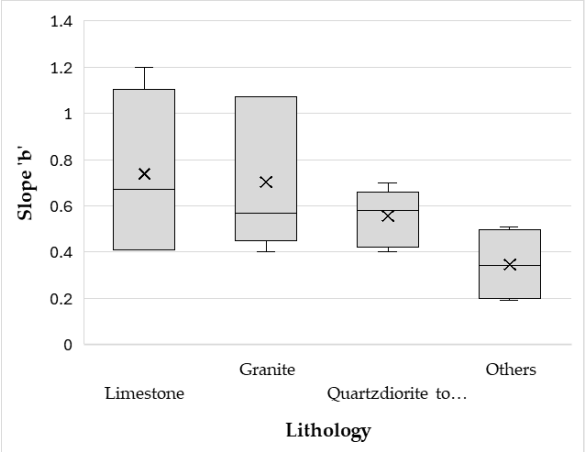

Figure 11. Site lithology vs slope 'b' for historical inventories.

Based on the change detection case studies (Table 4), limestone and sandstone represent the only lithologies with sufficient data to be treated as distinct categories. The group labeled "Others" comprises a variety of rock types; however, the number of case studies for each of these lithologies is too limited to justify separate classification. This highlights a limitation of the current dataset, where insufficient representation of certain lithologies restricts detailed lithology-specific analysis. The small sample size within the 'Others' category reduces statistical robustness and limits direct comparison with more well represented lithologies.

Table 4. Number of Change Detection studies b-value and rockfall events for each Lithology.

Rockfall Events	Limestone	Sandstone	Others [1]
	0.75	0.43	1
	0.682	0.663	1.01
	0.463	0.555	0.922
	0.676		0.54
Total	493	692	11,309

[1] The group "Other" represents the slope lithologies of basaltic cliffs ([27]), quartzofeldspathic gneiss ([35]), granodiorites ([40]), and upper cretaceous chalk ([41]).

Figure 12 presents the relationship between site lithology and the power-law slope b derived from change detection-based rockfall inventories. Only three lithological groups are represented in the change detection dataset: limestone, sandstone, and a composite group labeled "Others." The results indicate that limestone- and sandstone-dominated slopes exhibit relatively narrow and well-defined distributions of b-values, suggesting consistent frequency–magnitude behavior captured by the change detection method. For limestone, b-values range approximately from 0.45 to 0.75, while sandstone shows a similarly constrained range of about 0.4 to 0.65, with both distributions appearing relatively symmetric and homogeneous.

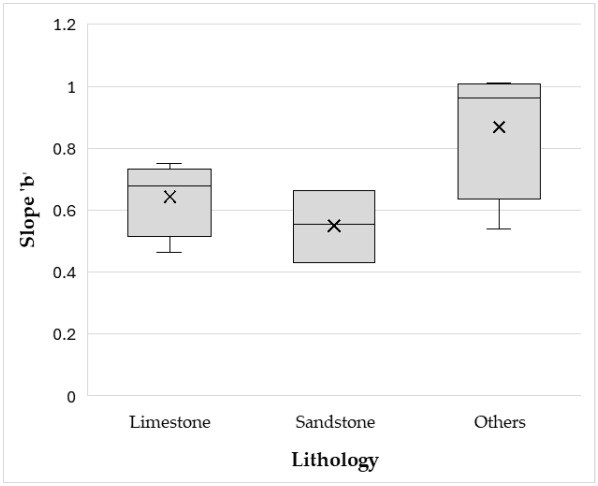

Figure 12. Site lithology vs slope 'b' for obtained from change detection.

The median and mean b-values for limestone are slightly higher than those for sandstone, indicating a greater relative contribution of small-volume rockfall events in limestone slopes compared to sandstone under the monitored conditions. In contrast, the "Others" category—which includes lithologies such as basaltic cliffs and granodiorites—exhibits a wider range and greater dispersion of b-values. This broader spread reflects the inherent heterogeneity in rock mass characteristics across these lithologies. While this aggregation is necessary for statistical power, it may obscure lithology-specific nuances, warranting further high-resolution investigation as more data becomes available.

The lithology-based analysis of historical rockfall inventories shows substantial variability and wide dispersion in b-values across rock types, reflecting strong observational bias and inconsistent detection of small-volume events. This variability limits the reliability of lithology–hazard relationships derived solely from historical data. In contrast, preliminary visual inspection suggests that change detection-based inventories yield more constrained and consistent b-value distributions for dominant lithologies, enabling clearer differentiation of lithological controls on rockfall behavior and providing more robust input for quantitative hazard assessment.

5.2. Power-Law Distribution—Historical vs. Change Detection Data

Figure 13 compares the distribution of power-law slopes (b-values) derived from rockfall volume–cumulative frequency curves using change detection inventories and historical records. Change detection data exhibit a higher median b of approximately 0.7 and a relatively narrow interquartile range of 0.45–0.9 for a total of 12,494 rockfall events. In contrast, historical inventories (total of 4059 rockfall events) show a lower median b of 0.5 and a substantially wider spread of 0.3–0.9, with values ranging from 0.2 to 1.2. This larger variability suggests that historical datasets are more strongly influenced by observational bias and heterogeneous data quality. However, this could be influenced by the limited number of case studies. Expanding the number of datasets through further research will help overcome this limitation and enable more robust analyses as data availability increases. Statistical analysis using the Mann–Whitney U test (p-value = 0.18) was performed on b-values taken from the original log–log plots. Although these statistical analyses are not adequate for small sample sizes, the p-value suggests that the observed differences are not yet statistically significant at the 0.05 level.

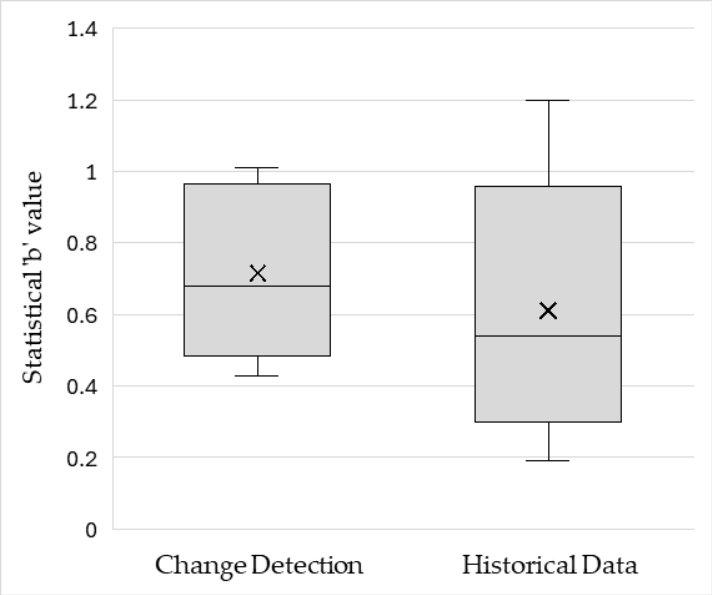

Figure 13. Statistical analysis of change detection and historical investigations.

Overall, the box plot suggests that change detection methods potentially yield more stable and typically higher b-values, supporting their use for robust estimation of rockfall frequency–magnitude relationships and hazard characterization.

5.3. Rollover

The power-law exponent (b-value) was calculated for the portion of the distribution exceeding the lower truncation limit. This limit, or rollover point, in both datasets was identified as the threshold of an approximate volume range, where the observed deviation of the RVC relationship from linearity in the log(volume)–log(cumulative frequency) space signifies the limit of inventory completeness. This threshold was selected to ensure that the subsequent b-value estimates were derived only from the statistically complete portion of the dataset. This empirical approach is consistent with established practices for power-law fitting in geomorphological datasets [48]. The lower and upper bounds of these volumes were then used to assess the influence of rockfall record sources (historical from observations or based on change detection techniques) on the volume where the rollover is observed as this can have a significant influence in rockfall hazard assessments. In Table 5 an approximate volume range of rollover effects alongside the total number of rockfall events for each record source is represented. The 'rollover effect' is significantly reduced in the change detection dataset. This is evidenced by the significantly larger sample size (N = 12,494), where the majority of additional events are concentrated in the 10^{-4}–10^{-2} m^3 range, which are typically underrepresented in historical inventories (N = 4059). Statistical comparison of these volume ranges yielded a Mann–Whitney U value of 116 (p-value < 0.001), confirming a highly significant difference in the completeness thresholds. Although these statistical analyses are not adequate for small sample sizes, the p-value for the b-values taken from the original log–log plots indicates that while volume ranges differ, the scaling exponents remain statistically comparable. Figure 14 also compares the resulting volume ranges derived from change detection inventories and historical observations using box-plot statistics.

Table 5. Numbers of events and rollover effects on volume range for change detection and historical inventories.

Type of Observation	Total Number of Events	Approximate Rollover Volume Range (m^3)
Change Detection	12,494	8×10^{-4}–4
Historical Inventories	4059	10^{-3}–10^{3}

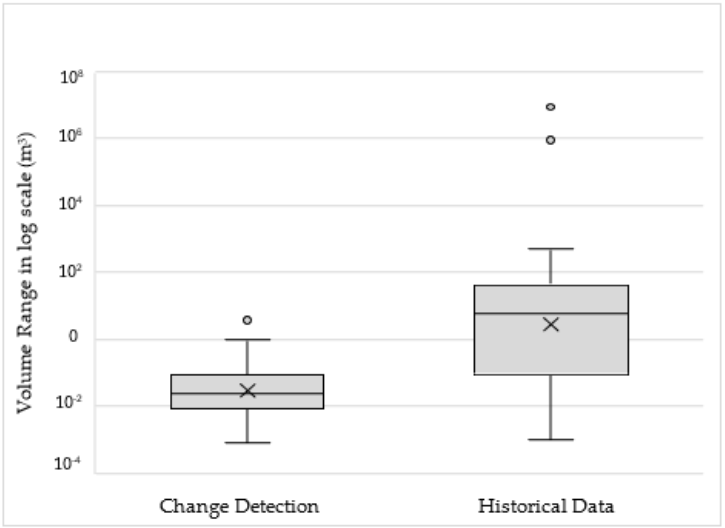

Figure 14. Rollover effects on historical and change detection dataset.

The box plot indicates that the change detection dataset is characterized by a lower and more constrained volume range, with a relatively homogeneous and consistent distribution of small-event volumes. The narrow interquartile range and limited whisker extent suggest reduced variability and minimal influence from extreme values, indicating effective capture of small magnitude rockfalls.

In contrast, historical inventories exhibit a markedly wider spread of volume ranges, spanning approximately from 10^{-3} m^3 to 10^3 m^3, with pronounced dispersion and heterogeneity. This broad range reflects substantial variability and suggests a bias toward larger, more easily observable events, consistent with censoring and underrepresentation of small rock slope failures.

6. Conclusions

The preliminary visual inspection suggests that change detection inventories yield more stable and higher b-values, underscoring their efficacy for robust frequency–magnitude estimation and hazard characterization. While these recent databases provide more detailed and less biased occurrence data, the findings are supported by Mann–Whitney U testing to quantify differences between inventory types. However, given the sample size constraints, these results are primarily presented as observational and exploratory to provide a foundational framework that can be further validated as future studies contribute additional case records to the global database.

In contrast, historical inventories exhibit greater variability and heterogeneity, reflecting strong observational bias and inconsistent detection of small-volume events. Similar trends are observed in lithological analysis, where change detection provides more consistent and comparable b-value estimates for dominant lithologies such as limestone and sandstone, while historical datasets show wider dispersion, particularly for heterogeneous or less-represented rock types. These findings highlight the strong influence of lithology on

rockfall volume–frequency behavior and underscore the limitations of historical inventories in reliably capturing small-magnitude events across different geological settings.

Overall, the results confirm that change detection offers a less biased and more comprehensive framework for constructing RVC curves and quantifying rockfall hazard. Although change detection methods cannot capture all rock slope failures, they are demonstrably less biased than traditional inventories. Their effectiveness is influenced by factors such as lighting conditions, visibility, weather, scan interval selection [35] and rock mass structure. When these factors are carefully managed, change detection enables the development of an improved and more reliable rockfall modeling database for rockfall hazard assessment compared to existing historical records.

Author Contributions: Conceptualization, S.B.; methodology, S.B.; formal analysis, S.B.; writing—original draft preparation, S.B.; supervision, R.M.; writing—review and editing, R.M. and S.B.; validation, R.M. and S.B. All authors have read and agreed to the published version of the manuscript.

Funding: This research was conducted with the support of (1) the (Canadian) Railway Ground Hazard Research Program (RGHRP), funded by the Natural Sciences and Engineering Research Council of Canada (NSERC), Canadian Railway Company (CN), Canadian Pacific Kansas City Railway (CPKC), and Transport Canada and (2) the highway geohazards research program supported by Alberta Transportation and Economic Corridors and funded by NSERC and Klohn Crippen Berger S.A, grant number, NSERC ALLRP 587029-23.

Data Availability Statement: The original contributions presented in this study are included in the article. Further inquiries can be directed to the corresponding author.

Acknowledgments: The authors would like to disclose that during the preparation of this manuscript, the authors used the artificial intelligence (AI) tool ChatGPT 5.2 for the purposes of grammatical corrections and improvement of sentence structure; no technical content, analysis, interpretations, or data were generated or derived using AI. The authors have reviewed and edited the output and take full responsibility for the content of this publication.

Conflicts of Interest: The authors declare no conflicts of interest.

References

1. Corominas, J.; Mavrouli, O.; Ruiz-Carulla, R. Magnitude and frequency relations: Are there geological constraints to rockfall size? *Landslides* **2018**, *15*, 829–845. [CrossRef]
2. Turner, A.K.; Jayaprakash, G.P. Introduction. In *Rockfall Characterization and Control*; Turner, A.K., Schuster, R.L., Eds.; Transportation Research Board, National Academy of Sciences: Washington, DC, USA, 2012; pp. 3–20.
3. Cruden, D.M.; Varnes, D.J. Landslide types and processes. In *Landslides Investigation and Mitigation*; National Research Council, Transportation Research Board: Washington, DC, USA, 1996; Volume Special Report 247, pp. 36–75.
4. Corominas, J.; Mavrouli, O.; Ruiz-Carulla, R. Rockfall occurrence and fragmentation. In *Advancing Culture of Living with Landslides*; Sassa, K., Mikos, M., Yin, Y., Eds.; Springer Nature: Cham, Switzerland, 2017; Volume 1, pp. 75–97. [CrossRef]
5. Guzzetti, F.; Reichenbach, P.; Ghigi, S. Rockfall hazard and risk assessment along a transportation corridor in the Nera Valley, central Italy. *Environ. Manag.* **2004**, *34*, 191–208. [CrossRef] [PubMed]
6. Read, J.; Stacey, P. *Guidelines for Open Pit Slope Design*; CRC Press/Balkema: Leiden, The Netherlands, 2009; p. 496.
7. Macciotta, R.; Altamirano, F.; Gibbins, L.; Espezua, M.; Fernández, R.; Maguiña, J. Rock fall hazard analysis for in-pit operations potentially impacting external sensitive areas. *Mining* **2021**, *1*, 135–154. [CrossRef]
8. Hungr, O.; Leroueil, S.; Picarelli, L. The Varnes classification of landslide types, an update. *Landslides* **2014**, *11*, 167–194. [CrossRef]
9. Hungr, O.; Evans, S.G.; Hazzard, J. Magnitude and frequency of rock falls and rockslides along the main transportation 475 corridors of southwestern British Columbia. *Can. Geotech. J.* **1999**, *36*, 224–238. [CrossRef]
10. Benjamin, J. Regional-Scale Controls on Rockfall Occurrence. Doctoral Dissertation, Durham University, Durham, UK, 2018. Available online: http://etheses.dur.ac.uk/12813/ (accessed on 27 November 2025).
11. Abellán, A.; Jaboyedoff, M.; Oppikofer, T.; Vilaplana, J.M. Detection of millimetric displacements using a terrestrial laser scanner: Experiment and application. *Eng. Geol.* **2011**, *119*, 7–14.
12. Rosser, N.J.; Lim, M.; Petley, D.N.; Dunning, S.A.; Allison, R. Patterns of precursory rockfall prior to slope failure. *JGR Earth Surf.* **2007**, *112*, F04014. [CrossRef]

13. Guerin, A.; Parsons, L.A.; Vick, L. Optimizing change detection workflows for rockfall monitoring using TLS. *Eng. Geol.* **2020**, *266*, 105450.
14. Corominas, J.; van Westen, C.; Frattini, P.; Cascini, L.; Malet, J.P.; Fotopoulou, S.; Catani, F.; Van Den Eeckhaut, M.; Mavrouli, O.; Agliardi, F.; et al. Recommendations for the quantitative analysis of landslide risk. *Bull. Eng. Geol. Environ.* **2014**, *73*, 209–263. [CrossRef]
15. Picarelli, L.; Oboni, F.; Evans, S.G.; Mostyn, G.; Fell, R. Hazard characterization and quantification. In *Landslide Risk Management*; Hungr, O., Fell, R., Couture, R., Eberthardt, E., Eds.; Taylor and Francis: London, UK, 2005; pp. 27–61.
16. Rossi, M.; Witt, A.; Guzzetti, F.; Malamud, B.D.; Peruccacci, S. Analysis of historical landslide time series in the Emilia Romagna region, northern Italy. *Earth Surf. Process. Landf.* **2010**, *35*, 1123–1137. [CrossRef]
17. Agliardi, F.; Crosta, G.B.; Frattini, P. Integrating rockfall risk assessment and countermeasure design by 3D modelling techniques. *Nat. Hazards Earth Syst. Sci.* **2009**, *9*, 1059–1073. [CrossRef]
18. Wang, X.; Frattini, P.; Crosta, G.B.; Zhang, L.; Agliardi, F.; Lari, S.; Yang, Z. Uncertainty assessment in quantitative rockfall risk assessment. *Landslides* **2014**, *11*, 711–722. [CrossRef]
19. Guzzetti, F.; Malamud, B.D.; Turcotte, D.L.; Reichenbach, P. Power-law correlations of landslide areas in Central Italy. *Earth Planet Sci. Lett.* **2002**, *195*, 169–183.
20. Guzzetti, F.; Reichenbach, P.; Wieczorek, G.F. Rockfall hazard and risk assessment in the Yosemite Valley, California, USA. *Nat. Hazards Earth Syst. Sci.* **2003**, *3*, 491–503. [CrossRef]
21. Malamud, B.D.; Turcotte, D.L.; Guzzetti, F.; Reichenbach, P. Landslide inventories and their statistical properties. *Earth Surf. Process. Landf.* **2004**, *29*, 687–711. [CrossRef]
22. Gutenberg, B.; Richter, C.F. *Seismicity of the Earth*, 2nd ed.; Princeton University Press: Princeton, NJ, USA, 1954.
23. Gardner, J. Rockfall: A geomorphic process in high mountain terrain. *Alta. Geogr.* **1970**, *6*, 15–20.
24. Dussauge-Peisser, C.; Grasso, J.R.; Helmstetter, A. Statistical analysis of rockfall volume distributions: Implications for rockfall dynamics. *J. Geophys. Res.* **2003**, *108*, 2286. [CrossRef]
25. Macciotta, R.; Cruden, D.M.; Martin, C.D.; Morgenstern, N.R.; Petrov, M. Spatial and temporal aspects of slope hazards along a railroad corridor in the Canadian Cordillera. In *Proceedings of the International Symposium on Slope Stability in Open Pit Mining and Civil Engineering, Slope Stability 2013*; Dight, P.M., Ed.; Australian Centre for Geomechanics: Perth, Australia, 2013. [CrossRef]
26. Chau, K.T.; Wong, R.H.C.; Liu, J.; Lee, C.F. Rockfall hazard analysis for Hong Kong based on rockfall inventory. *Rock Mech. Rock Eng.* **2003**, *36*, 383–408. [CrossRef]
27. Dussauge-Peisser, C.; Helmstetter, A.; Grasso, J.R.; Hantz, D.; Desvarreux, P.; Jeannin, M.; Giraud, A. Probabilistic approach to rock fall hazard assessment: Potential of historical data analysis. *Nat. Hazards Earth Syst. Sci.* **2002**, *2*, 15–26. [CrossRef]
28. Wieczorek, G.F.; Morrissey, M.M.; Iovine, G.; Godt, J. *Rock-Fall Hazards in the Yosemite Valley*; Open File Report; U.S. Geological Survey: Menlo Park, CA, USA, 1998.
29. Stark, C.P.; Hovius, N. The characterization of the landslide size distributions. *Geoph. Res. Lett.* **2001**, *28*, 1091–1094. [CrossRef]
30. Guthrie, R.H.; Evans, S.G. Analysis of landslide frequencies and characteristics in a natural system, Coastal British Columbia. *Earth Surf. Process. Landf.* **2004**, *29*, 1321–1339. [CrossRef]
31. Lim, M.; Rosser, N.J.; Allison, R.; Petley, D.N. Erosional processes in the hard rock coastal cliffs at Staithes, North Yorkshire. *Geomorphology* **2010**, *114*, 12–21. [CrossRef]
32. Pelletier, J.D.; Malamud, B.D.; Blodgett, T.; Turcotte, D.L. Scale-invariance of soil moisture variability and Its Implications for the Frequency-Size Distribution of Landslides. *Eng. Geol.* **1997**, *48*, 255–268. [CrossRef]
33. Jaboyedoff, M.; Oppikofer, T.; Abellán, A.; Derron, M.H.; Loye, A.; Metzger, R.; Pedrazzini, A. Use of LIDAR in landslide investigations: A review. *Nat. Hazards* **2012**, *61*, 5–28. [CrossRef]
34. Williams, J.G.; Rosser, N.J.; Hardy, R.J.; Brain, M.J.; Afana, A.A. Optimising 4D approaches to surface change detection: Improving understanding of rockfall magnitude–frequency. *Earth Surf. Dyn.* **2018**, *6*, 101–119. [CrossRef]
35. van Veen, M.; Hutchinson, D.J.; Kromer, R.; Lato, M.; Edwards, T. Effects of sampling interval on the frequency–magnitude relationship of rockfalls detected from terrestrial laser scanning using semi-automated methods. *Landslides* **2017**, *14*, 1579–1592. [CrossRef]
36. Guerin, A.; Hantz, D.; Rossetti, J.-P.; Jaboyedoff, M. Estimating rockfall frequency in a mountain limestone cliff using a terrestrial laser scanner. *Nat. Hazards Earth Syst. Sci.* **2014**, *2*, 123–135. [CrossRef]
37. Wollenberg-Barron, T.D.G.; Macciotta, R.; Mirhadi, N.; Gräpel, C.; Tappenden, K. Integrating Change Detection and Slope Assessment for Enhanced Rock Slope Asset Management. *Geotech. Geol. Eng.* **2024**, *42*, 7063–7083. [CrossRef]
38. Janeras, M.; Lantada, N.; Núñez-Andrés, M.A.; Hantz, D.; Pedraza, O.; Cornejo, R.; Guinau, M.; García-Sellés, D.; Blanco, L.; Gili, J.A.; et al. Rockfall Magnitude-Frequency Relationship Based on Multi-Source Data from Monitoring and Inventory. *Remote Sens.* **2023**, *15*, 1981. [CrossRef]

39. Carrea, D.; Abellan, A.; Derron, M.H.; Jaboyedoff, M. Automatic Rockfalls Volume Estimation Based on Terrestrial Laser Scanning Data. In *Engineering Geology for Society and Territory*; Lollino, G., Crosta, G.B., Corominas, J., Azzam, R., Wasowski, J., Sciarra, N., Eds.; Springer: Cham, Switzerland, 2015; Volume 2, pp. 425–428. [CrossRef]
40. Santana, D.; Corominas, J.; Mavrouli, O.; Garcia-Sellés, D. Magnitude–frequency relation for rockfall scars using a terrestrial laser scanner. *Eng. Geol.* **2012**, *145–146*, 50–64. [CrossRef]
41. Dewez, T.J.B.; Rohmer, J.; Regard, V.; Cnudde, C. Probabilistic coastal cliff collapse hazard from repeated terrestrial laser surveys: Case study from Mesnil Val (Normandy, northern France). *J. Coast. Res. JCR* **2013**, *65*, 702–707. [CrossRef]
42. Bolkas, D.; Walton, G.; Kromer, R.; Sichler, T. Registration of multi-platform point clouds using edge detection for rockfall monitoring. *J. Photogramm. Remote Sens. ISPRS* **2021**, *175*, 366–385. [CrossRef]
43. Huntley, D.; Bobrowsky, P.; Rotheram-Clarke, D.; MacLeod, R.; Cocking, R.; Joseph, J.; Holmes, J.; Donohue, S.; Chambers, J.; Meldrum, P.; et al. Protecting Canada's railway network using remote sensing technologies. In *Advances in Remote Sensing for Infrastructure Monitoring*; Springer International Publishing: Cham, Switzerland, 2020; pp. 81–109. [CrossRef]
44. Stead, D.; Donati, D.; Wolter, A.; Sturzenegger, M. Application of remote sensing to the investigation of rock slopes: Experience gained and lessons learned. *Int. J. Geo-Inf. ISPRS* **2019**, *8*, 296. [CrossRef]
45. Lato, M.J.; Hutchinson, D.J.; Gauthier, D.; Edwards, T.; Ondercin, M. Comparison of airborne laser scanning, terrestrial laser scanning, and terrestrial photogrammetry for mapping differential slope change in mountainous terrain. *Can. Geotech. J.* **2014**, *52*, 129–140. [CrossRef]
46. Van Westen, C.J.; Castellanos, E.; Kuriakose, S.L. Spatial data for landslide susceptibility, hazard, and vulnerability assessment: An overview. *Eng. Geol.* **2008**, *102*, 112–131. [CrossRef]
47. Lague, D.; Brodu, N.; Leroux, J. Accurate 3D comparison of complex topography with terrestrial laser scanner: Application to the Rangitikei canyon (N-Z). *J. Photogram. Remote Sens. ISPRS* **2013**, *82*, 10–26. [CrossRef]
48. Clauset, A.; Shalizi, C.R.; Newman, M.E.J. Power-law distributions in empirical data. *SIAM Rev.* **2009**, *51*, 661–703. [CrossRef]

Disclaimer/Publisher's Note: The statements, opinions and data contained in all publications are solely those of the individual author(s) and contributor(s) and not of MDPI and/or the editor(s). MDPI and/or the editor(s) disclaim responsibility for any injury to people or property resulting from any ideas, methods, instructions or products referred to in the content.